



Highly active iridium–rhenium catalyst condensed on silica support for hydrogenolysis of glycerol to 1,3-propanediol



Lujie Liu^a, Shota Kawakami^a, Yoshinao Nakagawa^{a,b,*}, Masazumi Tamura^{a,b}, Keiichi Tomishige^{a,b,*}

^a Department of Applied Chemistry, School of Engineering, Tohoku University, 6-6-07 Aoba, Aramaki, Aoba-ku, Sendai, 980-8579, Japan

^b Research Center for Rare Metal and Green Innovation, Tohoku University, 468-1, Aoba, Aramaki, Aoba-ku, Sendai 980-0845, Japan

ARTICLE INFO

Keywords:

Glycerol hydrogenolysis
1,3-Propanediol
Iridium
Rhenium
High loading amount

ABSTRACT

Increase of loading amount of Ir-ReO_x/SiO₂ catalyst up to 20 wt% of Ir enhanced the Ir-based activity in glycerol hydrogenolysis to 1,3-propanediol. The ratio of used precursor amount was set constant (Re/Ir = 1; “nominal” Re/Ir ratio); however, actual Re/Ir amount was lower at higher loading amount because of the loss of Re during calcination. The catalytic performance, reactivity of related substrates and kinetics over optimized Ir-ReO_x/SiO₂ (20 wt%-Ir, Re/Ir = 0.34, actual) was compared with the previously reported catalyst (4 wt%-Ir, Re/Ir = 1, nominal; Re/Ir = 0.83, actual) without H₂SO₄ addition which increases the activity and stability of 4 wt%-Ir Ir-ReO_x/SiO₂ catalyst. High 1,3-propanediol selectivity (ca. 70%) was obtained over 20 wt%-Ir Ir-ReO_x/SiO₂ at 20% conversion level of glycerol. This high selectivity was almost independent of glycerol concentrations, while 4 wt%-Ir Ir-ReO_x/SiO₂ catalyst showed lower selectivity when glycerol concentration was lower. The 20 wt%-Ir Ir-ReO_x/SiO₂ exhibited good reusability under optimized reaction conditions when recovered without exposure to air. Small Ir metal particles (~3 nm) were observed from both XRD and TEM regardless of high Ir loading amount. The results of XANES and EXAFS suggested high reduction degree of Re species (~80%); however, further characterization of XRD and CO FT-IR supported the absence of Ir-Re alloy. Combined with TPR and CO adsorption results, we proposed that ReO_x cluster at low average valence (ca. + 1~+2) was attached to Ir metal. This unique structure decreased the effect of SiO₂ support and increased the number of active sites, accounting for higher activity. The heterolytic dissociation of hydrogen molecule (~1 reaction order on H₂ pressure) and strong interaction between glycerol and catalyst surface (~0 reaction order on glycerol concentration around standard reaction conditions, 67 wt% glycerol solution) were suggested for 20 wt%-Ir Ir-ReO_x/SiO₂ catalyst. This 20 wt%-Ir Ir-ReO_x/SiO₂ catalyst can be also applied to various substrates with –O—C—CH₂OH structure for the selective cleavage of the C—O bond.

1. Introduction

Chemical transformation of biomass-derived glycerol to another value-added compound has received much attention, since glycerol is a low-cost feedstock for C3 functional chemicals [1,2]. At present, glycerol can be selectively converted into various valuable chemicals via many routes, including selective oxidation to produce glyceric acid [3], selective dehydration to obtain acrolein [4,5], selective hydrogenolysis to prepare 1,2-propanediol (1,2-PrD) [6–8] and 1,3-propanediol (1,3-PrD) [9–16], and aqueous phase reforming to produce H₂ [17,18]. Among these routes, glycerol hydrogenolysis to 1,3-propanediol is regarded as a promising way for industrial application and has been widely investigated due to the wide applications of 1,3-propanediol in

manufacture of polytrimethylene terephthalate, polyurethanes, and cyclic compounds [19,20]. However, it is still a great challenge for selective formation of 1,3-PrD since the reactivity of secondary hydroxyl group of glycerol is profoundly decreased by the steric hindrance effect [21]. Moreover, raw glycerol always contains some amount of water, and glycerol hydrogenolysis process will also lead to the by-product water formation. In some cases, the highly active catalyst showed relatively poor 1,3-PrD selectivity in water instead of using organic solvent, e. g. 12.3% yield of 1,3-PrD at 62.9% conversion in water compared to 55.6% yield of 1,3-PrD at 66.5% conversion over Pt on sulfated ZrO₂ catalyst in 1,3-dimethyl-2-imidazolidinone solvent [22]. Considering the economic and environmental advantages, it is of significance to develop further efficient catalytic systems in water

* Corresponding authors at: School of Engineering, Tohoku University, 6-6-07, Aoba, Aramaki, Aoba-ku, Sendai, 980-8579, Japan.

E-mail addresses: yoshinao@erec.che.tohoku.ac.jp (Y. Nakagawa), tomi@erec.che.tohoku.ac.jp (K. Tomishige).

solvent.

Generally, an efficient catalyst for 1,3-PrD production by glycerol hydrogenolysis requires noble metals (Pt, Ir, Rh) for activation of H₂ molecules and oxophilic promoters (WO_x, ReO_x, MoO_x) for activation of the secondary hydroxyl group [23]. Up to now, the Pt-WO_x based and Ir-ReO_x based catalytic systems give the best performance in terms of 1,3-PrD yield using water as a solvent. García-Fernández and co-workers reported a selectivity towards 1,3-PrD of 51.9% at 53.1% conversion over Pt/WO_x/Al₂O₃ at 4.5 MPa H₂ and 473 K for 24 h [12]. Later, they investigated the support effect of Pt-WO_x catalysts, and found the density of surface W and interaction between Pt and WO_x were of the essence in 1,3-PrD formation [24]. The Pt/WO₃-Al₂O₃-SiO₂ catalysts gave about 56% 1,3-PrD selectivity at 48% conversion at 6 MPa H₂ and 433 K for 12 h [25]. Zhu and co-workers has made many efforts in selective hydrogenolysis of glycerol. They obtained a selectivity of 48.1% to 1,3-PrD at 24.1% conversion over the Pt-H₄SiW₁₂O₄₀/ZrO₂ catalyst [26], and achieved a higher yield of 1,3-PrD (53.6% selectivity at 43.5% conversion) by employing Li-modified Pt-H₄SiW₁₂O₄₀/ZrO₂ catalyst at 5 MPa H₂ and 453 K in a fixed-bed reactor [27]. To make a forward step, the same group developed SiO₂ promoted Pt/WO_x/ZrO₂ catalysts. They proposed a dehydration-hydrogenation reaction mechanism, and the maximum selectivity to 1,3-propanediol was 52.0% at 54.3% conversion at 5 MPa H₂ and 453 K over the catalyst with modification of 5.0 wt% of SiO₂ [11]. Up to date, the highest 1,3-PrD yield (66–69%) was achieved by employing Pt/WO_x/AlOOH catalyst using boehmite (AlOOH) support to disperse tungsten(VI) oxide species [9]. The number of Al-OH species was accounted for the high performance of this catalyst. Recently, Qiao et al. found the crystal phase of zirconia significantly affected the catalytic activity [28]. Sequentially deposition of Pt and WO_x on tetragonal ZrO₂ (*t*-ZrO₂) support exhibited excellent performance rather than using monoclinic ZrO₂ (*m*-ZrO₂) as a support. High 1,3-PrD yield of 49.4% was obtained over Pt-WO_x/*t*-ZrO₂ catalyst at 8 MPa H₂ and 413 K for 24 h. The smaller Pt particles with better synergy and more Brønsted acid sites serving as formation of suitable intermediate of 1,3-PrD were responsible for the superiority in glycerol hydrogenolysis to 1,3-PrD. More recently, Ma and co-workers found that the moderately polymerized WO_x species over Pt/WO_x/ZrO₂ favored the 1,3-PrD formation, and the turnover frequency (TOF) was increased by 2.6 times by addition of appropriate amount of Mn on Pt/WO_x/ZrO₂ because of the promotion of the medium polymerization degree of WO_x species [29]. In most cases, the Pt-W based catalysts require high loading amount of tungsten to improve selectivity of 1,3-PrD [30]. However, Qiao et al. proposed that Pt/W-SBA-15 catalyst with low contents of tungsten (Pt: 3.0 wt%, W/Pt molar ratio = 0.16) gave high 1,3-PrD selectivity of 70.8% at 86.8% conversion under temperature of 423 K and 4 MPa H₂ for 30 h [31].

We firstly reported the Rh-ReO_x/SiO₂ (Rh: 4 wt%, Re/Rh = 0.5, nominal molar ratio) catalyzed glycerol hydrogenolysis. This system works effectively even at the low reaction temperature (~393 K), and maintains high propanediols selectivity, although the obtained 1,3-PrD selectivity (~20%) was less than satisfactory [14,32]. Soon afterwards, the Ir-ReO_x/SiO₂ (Ir: 4 wt%, Re/Ir = 1, nominal molar ratio) catalyst was discovered [13] and fully investigated [15,33–36], and it gave high 1,3-PrD selectivity (67 ± 3%) at initial stage in glycerol hydrogenolysis [13]. The 1,3-PrD yield reached 38% at a high glycerol conversion of 81% with sulfuric acid addition at 8 MPa H₂ and 393 K for 36 h. However, this system is assisted by sulfuric acid, and the activity becomes lower (ca. half) without sulfuric acid [15]. The role of sulfuric acid in glycerol hydrogenolysis has been concluded as stabilizing the catalytically active site [15]. Since the drawback of using sulfuric acid has limited the development and application of this system, various solid acids were applied to replace the sulfuric acid by utilizing the co-catalyst [33]. The H-ZSM-5 was regarded as an alternative co-catalyst for Ir-ReO_x/SiO₂ + H₂SO₄ at the expense of the maximum 1,3-PrD yield. Since the high activity in C–O hydrogenolysis over Ir-ReO_x/SiO₂, the wide application has been attempted using this catalyst in selective

hydrogenolysis of various molecules, including alcohol [13,15,33,34,36], cyclic ethers with OH groups [35], erythritol [37], sugars, and sugar alcohols [38–41]. Ir-ReO_x/SiO₂ catalyst can be also applied to selective hydrogenation to unsaturated alcohols [42,43], and total hydrodeoxygenation to prepare alkanes for transportation fuel [44–46], and those for lubricants [47].

On the other hand, strong metal-oxide interaction (SMOI) has been exploited in development of metal catalysts by direct modification with metal oxide promoter [48–50]. In this article, we report that the support-metal oxide interaction rather decreases Ir-ReO_x interaction. Preparation of high loading Ir-ReO_x pairs with retention of good dispersion further decreases the effect of SiO₂ support. The 20 wt%-Ir Ir-ReO_x/SiO₂ (Re/Ir = 1, nominal molar ratio) gave high activity and maintained high 1,3-PrD selectivity (ca. 70%) at the initial stage without H₂SO₄ addition. The reactivity of related substrates, catalyst structure and reaction kinetics were also compared using this catalyst and 4 wt%-Ir-ReO_x/SiO₂ to clarify the superiority of 20 wt%-Ir Ir-ReO_x/SiO₂. The reusability was also confirmed under optimized operation conditions. In addition, pre-reduction method of catalyst and various metal-oxide modifiers were also discussed.

2. Experimental

2.1. Catalysts preparation

The support of SiO₂ (Fuji Silysia, G-6) was pre-calcined at 973 K for 1 h. The BET surface area was 485 m² g⁻¹. Impregnation method was used for preparing Ir-ReO_x/SiO₂ catalyst as the previous report [15]: SiO₂ was firstly impregnated with H₂IrCl₆ aqueous solution. The sample was dried at 383 K for 12 h after evaporating the solvent. Afterwards, the Ir/SiO₂ was further impregnated with NH₄ReO₄ aqueous solution. After drying for 12 h at 383 K, the catalyst was subsequently calcined at 773 K for 3 h. For Ir-MO_x/SiO₂ (M represents for transition metal) catalysts, same preparation method was used. The precursors employed were summarized in Table S1. The Ir loading amount varied, and an additive amount was based on constant molar ratio of additive to Ir (typically 1). As described later, the actual loading amount was different from the intended value because of the sublimation of rhenium oxide during calcination. The intended value is called as “nominal” one in this paper. Unless noted as “nominal”, the Re/Ir value of the catalysts in this paper is the actual one determined by characterization.

2.2. Activity tests

A stainless steel autoclave (190 ml) was used for activity test. First, the catalyst and water solvent were added to glass inner vessel. The vessel was set to the reactor, and then the reactor was purged with 1 MPa H₂ three times. After that, 8 MPa H₂ was introduced into the autoclave and temperature was increased to 473 K for reduction pre-treatment for 1 h. The Ir-ReO_x/SiO₂ catalysts reduced in liquid-phase at 473 K were denoted as Ir-ReO_x (L, 473). After cooling down and depressurizing, glycerol was quickly added into the autoclave. In some cases, a desired amount of diluted sulfuric acid or Re₂O₇ dissolved in water was added. Same procedures were performed to remove the air as described above. Once the temperature was increased to 393 K (reaction temperature), the reactor was pressurized with H₂ rapidly to 8 MPa and defined as 0 h. The mass transfer effects were eliminated at fixed stirring rate of 500 rpm. After reaction, a gas bag was used to collect gas-phase products for analysis using gas chromatograph (Shimadzu GC-2025). Liquid-phase products for GC test were collected after separation from the rest of the reaction mixture. GC-MS (QP5050, Shimadzu) was further used to identify all the products. The standard reaction was carried out in the following conditions: initial hydrogen pressure at 8.0 MPa, reaction temperature at 393 K, reaction time for 4 h, 4 g (43 mmol) of glycerol, 2 g of water, and 150 mg of 4 wt%-Ir Ir-ReO_x/SiO₂ (Re/Ir = 1, nominal) or 30 mg of 20 wt%-Ir Ir-ReO_x/SiO₂

(Re/Ir = 1, nominal) catalyst to keep the total amount of Ir metal constant (6 mg, 31 µmol). Some of the parameters were adjusted to examine the effect of reaction conditions, and the details can be found in each figure or table. For those kinetic results, the glycerol conversion rate was calculated based on the slope of initial three points at conversion lower than 25%. Our previous work suggested that suitable reduction conditions for Re-Pd/SiO₂ affected the activity in hydrogenation of stearic acid and dicarboxylic acid significantly [51,52]. Different reduction degree of Re species was accomplished using liquid-phase or gas-phase reduction treatments, resulting in different catalytic performance. Therefore, catalysts reduced by gas-phase flowing hydrogen at higher reduction temperature were also investigated. These samples were denoted similarly to the liquid-phase reduced catalysts. For instance, Ir-ReO_x (G, 473) represents for catalyst reduced under hydrogen flow (100% H₂, 30 mL min⁻¹) using a glass tube at 473 K for 1 h. The gas-phase reduced catalysts at 473, 773 or 973 K were prepared, and they were added into the reactor under N₂ atmosphere to avoid exposure to air. Subsequently, same procedure (purging N₂ with 1 MPa H₂, heating, and pressurizing with 8 MPa H₂) for the activity test was carried out as described above.

The main products were 1,3-PrD and 1,2-PrD after glycerol hydrogenolysis, and the overhydrogenolysis products included propanols (2-PrOH and 1-PrOH) and propane. Others referred to the C-C cracking products, propane and degradation products. The hydrogenolysis of related substrates, like 1,3-PrD, 1,2-PrD, ethylene glycol, 2-butoxyethanol, 2-ethoxyethanol, 2-isopropoxyethanol, and 1-methoxy-2-propanol was also compared by using 4 wt%-Ir and 20 wt%-Ir Ir-ReO_x/SiO₂ catalysts. The conversion and the selectivity were calculated on the carbon basis as previous report [13,15]. The carbon balance in each result was within the experimental error ($\pm 10\%$), indicating no formation of polymeric by-products. The 1,3-PrD productivity ($P_{1,3-\text{PrD}}$) was defined as: $P_{1,3-\text{PrD}} = (\text{Initial moles of glycerol} \times \text{Yield}_{1,3-\text{PrD}} \times 76 \text{ g mol}^{-1}) / (\text{total Ir amount (g)} \times \text{reaction time (h)})$. TOF was evaluated on the basis of surface Ir metal, which is determined from CO adsorption data (catalyst pre-reduced in gas phase, Section 2.3), and it is defined as the following equation: $\text{TOF (CO)} = \text{amount of converted substrate (mol)} / \{\text{dispersion (based on CO adsorption amount [CO]/[Ir])} \times (\text{total Ir amount (mol)}) \times \text{reaction time (h)}\}$. Conversion rate of glycerol was calculated by the equation: $\text{amount of converted glycerol (mmol)} / (\text{catalyst amount (g)} \times \text{reaction time (h)})$.

Two approaches were used to investigate the reusability of these catalysts. One method was to collect the 4 wt%-Ir and 20 wt%-Ir Ir-ReO_x/SiO₂ catalysts after reaction by centrifugation without washing. After drying at 383 K in air for 12 h and calcination at 773 K for 3 h, catalysts were pre-reduced in liquid phase as the standard reaction procedure before each reuse test. The loss of 4 wt%-Ir Ir-ReO_x/SiO₂ catalyst was compensated with fresh catalyst during the recovery process. The leaching amount after reuse test was obtained by filtration under N₂ atmosphere and measured by inductively-coupled plasma atomic emission spectrometry (ICP-AES, ThermoFisher iCAP6500, detection limit for both Ir and Re < 1 ppm). The other reuse method is as follows. Before the reuse test, catalyst was reduced in liquid phase (L, 473). After reaction, separated catalyst by decantation was directly introduced to the autoclave for the next test under N₂ atmosphere without further reduction treatment. The amount of glycerol and water solvent in each reuse was adjusted to keep the glycerol/water/catalyst ratio.

2.3. Catalyst characterization

Thermogravimetric (TG) curves were obtained using a Shimadzu TGA-DTA-50 analyzer. Approximately 11 mg of catalyst after drying was used, and then it was heated from 300 to 1100 K at a rate of 10 K/min under air atmosphere. The accurate loading amount of Ir and Re was measured on a wavelength dispersive X-ray fluorescence (XRF) instrument (Bruker, S8 Tiger) under He atmosphere. About 0.8 g of calcined

catalyst was mixed with ZrO₂ (0.2 g, internal standard), and calibration curve was determined by using commercial IrO₂ and ReO₂.

Temperature-programmed reduction (TPR) patterns were recorded to determine the reducibility of Ir-ReO_x/SiO₂ under diluted hydrogen flow (5% H₂/Ar, 30 mL min⁻¹). About 30–50 mg of catalyst was loaded in a fixed-bed reactor, and it was heated from ambient temperature to 800 K at 10 K/min. The effluent was dried with frozen acetone and analyzed by TCD. X-ray diffraction (XRD) patterns were obtained on a Rigaku MiniFlex600 diffractometer. In the case of XRD patterns obtained without exposure to air, catalysts were recovered and loaded on an *in-situ* cell under N₂ atmosphere, and Si powder was mixed as an internal standard to check the shift of diffraction peak of Ir metal. Scherrer equation was used to calculate the average particle size [53]. The Transmission electron microscope (TEM) images of catalysts were taken by HITACHI HF 2000EDX instrument. For TEM measurement, catalysts after reaction were collected, dispersed in ethanol solvent, transferred on Cu grids, and dried in the air. Average particle size was calculated by $\Sigma n_i d_i^3 / \Sigma n_i d_i^2$ (d_i : particle size; n_i : number of particle with size d_i) [54]. A volumetric method was used to acquire the CO chemisorption amount in a home-made high-vacuum system. Prior to CO adsorption, catalyst (0.15 and 0.05 g for 4 wt%-Ir and 20 wt%-Ir Ir-ReO_x/SiO₂, respectively) was reduced (473 K for 1 h), and then it was cooled to ambient temperature for measurement. The gas pressure (pure CO) was around 1.2 kPa after adsorption. In some cases, the wet form catalyst after liquid-phase reduction or after reaction was dried in N₂ atmosphere, and directly transformed to the measurement tube without further reduction. The number of CO adsorption was assumed to be equal to that of the surface Ir atoms and the dispersion of Ir was represented as CO/Ir.

The X-ray absorption near edge structure (XANES) and extended X-ray absorption fine structure (EXAFS) spectroscopy was conducted, and specific description of measurement and analysis is shown in supplementary material. Regard to the sample preparation, about 50 mg of catalyst after calcination was firstly diluted with 100 mg of SiO₂ to make uniform disks. For the gas-phase reduced catalyst, the sample disk was reduced (473 K for 1 h) in H₂ flow and was packed in a plastic bag under N₂ atmosphere. The thickness of the sample disks was about 2 mm, and the edge jump for Ir L₃-edge and Re L₃-edge was 0.8 and 0.2, respectively. The edge jumps agreed with the actual Re/Ir ratio (0.34) rather than the nominal one (1). For the catalyst after the catalytic use, autoclaves were opened under nitrogen atmosphere. About 120 mg of the sample after standard reaction conditions was mixed with 100 mg of SiO₂, and then it was introduced to the measurement cell. The thickness of the cell was also about 2 mm, and the edge jump for Ir L₃-edge and Re L₃-edge measurement was 1.2 and 0.4, respectively. The XANES and EXAFS data were recorded using a transmission mode. FT-IR spectra of adsorbed CO were measured in an *in-situ* cell with transition mode by Nicolet 6700 FT-IR. Catalysts (30 mg) were diluted with 20–80 mg of SiO₂ and pressed into a disk with about 20 mm diameter. The disk was reduced (473 K for 1 h) with H₂ in the IR cell, and the cell was evacuated and cooled down. The adsorption gas (6.7 kPa CO) was flowed into the system and circulated for 1 h to reach saturation. The FT-IR spectra were acquired after removing the rest of CO. The spectra of reduced catalysts without exposing to CO were subtracted from the raw spectra.

3. Results and discussion

3.1. Effect of Ir loading amount on glycerol hydrogenolysis without H₂SO₄ addition

The performance of Ir-ReO_x/SiO₂ with different Ir loading amount is presented in Fig. 1. The Re/Ir ratio of the impregnated precursor amount was 1 (Re/Ir = 1, nominal); however, as discussed later (Section 3.3), the actual Re amount was lower because of the sublimation of Re oxide during calcination, especially when the loading amount was

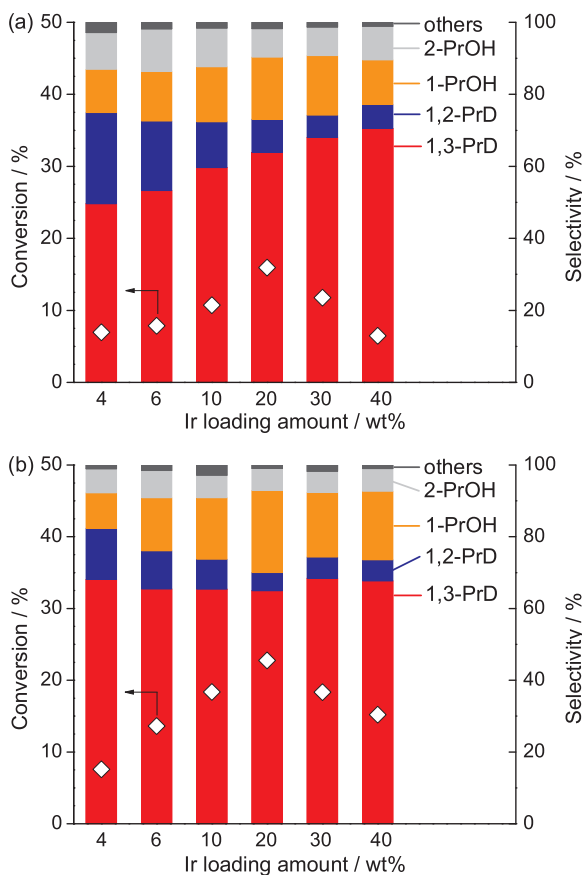


Fig. 1. Catalytic performance of the Ir-ReO_x/SiO₂ catalyst with nominal Ir loading amount varied from 4 wt% to 40 wt%. Re/Ir ratio of the impregnated precursor amount was 1 (nominal Re/Ir ratio), and the actual Re/Ir ratio is shown in Table 2. Reaction conditions: (a) 5 wt% glycerol solution (glycerol = 2 g (22 mmol), H₂O = 38 g), (b) 67 wt% glycerol solution (glycerol = 4 g (43 mmol), H₂O = 2 g), catalyst amount varied from 15 to 150 mg (Ir amount = 6 mg (31 μmol)) when the actual Ir amount was equal to nominal value, P(H₂) = 8 MPa, T = 393 K, t = 4 h. Reduction conditions: reduction temperature 473 K, reduction time 1 h, H₂ pressure 8 MPa. PrD, propanediol; PrOH, propanol. Others: ethylene glycol + ethanol + propane + ethane + methane.

high. Two concentrations of glycerol (low: 5 wt%; high: 67 wt%) were tested, since we have reported that high glycerol concentration is necessary to obtain high 1,3-PrD selectivity over 4 wt%-Ir Ir-ReO_x/SiO₂

catalyst [13,15]. The amount of catalyst was set to keep the nominal Ir amount constant (6 mg, 31 μmol). In low glycerol concentration (5 wt% glycerol solution, Fig. 1(a)), the glycerol conversion showed a volcano-type dependence on the nominal Ir loading amount. The activity was much enhanced with increasing Ir loading amount from 4 wt%, and reached a maximum at 20 wt%. As regard to product distribution, the selectivity of 1,3-PrD + 1,2-PrD almost unchanged, and 1,3-PrD selectivity gradually increased with decreasing the 1,2-PrD formation at Ir loading amount from 4 wt% to 40 wt%. The 1,3-PrD selectivity was higher than 60% over ≥ 20 wt%-Ir Ir-ReO_x/SiO₂ catalyst, while 4 wt% Ir-ReO_x/SiO₂ catalyst gave this high selectivity only in high glycerol concentration. The conversion tendency of glycerol in high concentration (67 wt% glycerol solution, Fig. 1(b)) was almost the same. When the Ir loading amount was between 4 wt% and 20 wt%, the glycerol conversion increased with increasing Ir loading amount. The conversion decreased when Ir loading amount exceeded 20 wt%. The selectivity of 1,3-PrD maintained at 66 ± 2% regardless of Ir loading amount screened in high glycerol concentration. The glycerol conversion and 1,3-PrD selectivity over 20 wt%-Ir Ir-ReO_x/SiO₂ (65% selectivity at 23% conversion) was comparable to the reported 4 wt%-Ir Ir-ReO_x/SiO₂ + H₂SO₄ system under the same reaction conditions (1,3-PrD selectivity of 59% at 22% conversion) [15]. In order to clarify the promoting effect with high Ir loading amount, 4 wt%-Ir and 20 wt%-Ir Ir-ReO_x/SiO₂ (Re/Ir = 1, nominal) catalysts were selected for comparison.

3.2. Effect of the catalyst composition on glycerol hydrogenolysis

We have reported that the additive amount of Re affected the catalytic activity of Ir-ReO_x/SiO₂ significantly in glycerol hydrogenolysis [15]. For 4 wt%-Ir catalysts, reaction rate is low at low ratio of Re to Ir. The activity is increased almost linearly up to Re/Ir = 1 (nominal), and then gradually increased up to Re/Ir = 2 (nominal). The catalytic performance of 20 wt%-Ir Ir-ReO_x/SiO₂ with various Re additive amount is presented in Table 1. The activity increased with the increase of Re amount. To compare the selectivity, the reaction time for Re/Ir = 0.5 and 1 (nominal) catalysts was adjusted to obtain 30–40% conversion level. The 1,3-PrD selectivity was similar for all Re/Ir = 0.5, 1 and 2 (nominal) catalysts. Considering the high cost of Re, we selected Re/Ir = 1 (nominal) catalyst for the following studies. On the other hand, almost no activity was observed over high loading amount of Ir/SiO₂ and ReO_x/SiO₂ in glycerol hydrogenolysis, which was similar to the case of 4 wt% Ir/SiO₂ and ReO_x/SiO₂ catalysts [14,15]. As a result, the glycerol hydrogenolysis also proceeded at the interface between Ir and ReO_x over 20 wt%-Ir Ir-ReO_x/SiO₂.

In the reported catalytic system (4 wt%-Ir Ir-ReO_x/SiO₂ + H₂SO₄)

Table 1
Glycerol hydrogenolysis over 20 wt% Ir/SiO₂, 20 wt%-Ir Ir-ReO_x/SiO₂ with different molar ratio of Re to Ir and ReO_x/SiO₂.

Catalyst	Re/Ir molar ratio		React. time / h	Conv./ %	Selectivity / %					1,3-PrD yield / %
	nominal ^a	actual ^b			1,3-PrD	1,2-PrD	1-PrOH	2-PrOH	Others	
20 wt% Ir/SiO ₂	0	–	24	< 1	30	66	–	5	–	< 0.1
20 wt%-Ir Ir-ReO _x /SiO ₂	0.5	0.22	4	12	73	5	16	6	1	9
	1	0.34	4	23	65	5	23	6	1	15
	2	0.37	4	33	59	5	29	6	2	19
	0.5	0.22	24	37	63	6	22	7	1	22
	1	0.34	8	36	60	5	26	7	2	21
	1	0.55	4	13	60	14	16	9	1	8
20 wt%-Ir Ir-ReO _x /SiO ₂ ^a	1	(19.4 wt%) ^{b,c}	24	< 1	43	57	–	–	–	< 0.1

Reaction conditions: 20 wt%-Ir Ir-ReO_x/SiO₂ = 30 mg, 67 wt% glycerol solution (glycerol = 4 g (43 mmol), H₂O = 2 g), P(H₂) = 8 MPa, T = 393 K. Reduction conditions: reduction temperature 473 K, reduction time 1 h, H₂ pressure 8 MPa. PrD, propanediol; PrOH, propanol. Others: ethylene glycol + ethanol + propane + ethane + methane.

^a Calcined at 673 K for 3 h.

^b Determined from XRF analysis.

^c Loading amount of Re.

for glycerol hydrogenolysis, various transition metals M (M represents W, Mo, V, Cr, Mn and Ag; M/Ir = 0.25, nominal) have been also tested as an additive [15]. Re, Mo and W were effective promoters, and Re was by far the best promoter, while other transition metals (Cr, Mn, V and Ag) were not effective. The glycerol conversion and 1,3-PrD selectivity were decreased as follows: Ir-ReO_x > Ir-MoO_x > Ir-WO_x and Ir-ReO_x > Ir-WO_x > Ir-MoO_x, respectively. Herein, various additives to high loading amount Ir/SiO₂ were also tested. The catalysts with additive/Ir a ratio of 1 (nominal) were compared first (Fig. S1). Similarly to 4 wt% Ir/SiO₂ cases, V, Cr, Mn, Ag, Co, Ni and Cu were not effective promoters. For Re, Mo and W as promoters, the activity order was Re > Mo > W, and the 1,3-PrD selectivity order was Re > Mo ≈ W. For Mo promoter, the addition amount (Mo/Ir ratio) was optimized (Fig. S2). Even the optimized Ir-MoO_x/SiO₂ catalyst (Mo/Ir = 0.25, nominal molar ratio), the performance was still much lower than Ir-ReO_x/SiO₂. Accordingly, high loading amount Ir-ReO_x/SiO₂ exhibited the best performance.

3.3. Loss of Re species during calcination

Re₂O₇ can sublime at high temperature, and the loading amount of calcined catalysts can be different from the calculated precursor amount. The actual loading amount of Ir-ReO_x/SiO₂ catalysts after calcination was determined by XRF, and the results are listed in Table 2. The accurate Re/Ir ratio decreased rapidly with increasing the Ir loading amount on Ir-ReO_x/SiO₂ catalysts (Re/Ir = 1, nominal), and actual Re/Ir ratio was much lower than the nominal one on high loading amount Ir-ReO_x/SiO₂ catalysts (Table 2). For ReO_x/SiO₂ (Re: 19.4 wt%, nominal) catalyst after calcined at 773 K, only 8.4 wt% of Re was actually loaded on SiO₂ support. The 20 wt%-Ir Ir-ReO_x/SiO₂ (Re/Ir = 1, nominal) after calcination gave a much lower Re/Ir ratio (0.34) than the nominal value (1) while the actual Ir loading amount (19.8 wt %) was almost the same as the nominal one (20 wt%, Table 2). While for 4 wt%-Ir Ir-ReO_x/SiO₂ (Re/Ir = 1, nominal), the loss of Re was not severe, and the accurate loading amount (Ir: 3.9 wt%, Re: 3.2 wt%, Re/Ir = 0.83) is close to the nominal loading amount (Table 2). Therefore, we tested the catalyst calcined at lower temperature (673 K) than the standard (773 K). The Ir loading amount was the same (19.8 wt% Ir, Table 2), and the Re amount increased (Re/Ir = 0.55) compared to that of the catalyst calcined at 773 K (Re/Ir = 0.34). However, the activity decreased significantly (ca. half, Table 1). Probably, the decomposition of Ir precursor (H₂IrCl₆) was not complete since the total decomposition of Ir precursor to IrO₂ occurred at the temperature around 773 K based on TG measurement (Fig. S3). In spite of the large loss of Re in the current preparation method, the low actual amount of Re in the highly active catalyst gives us hope that more inexpensive catalyst will be developed in the future.

Table 2

Loading amount of Ir and Re on SiO₂ support determined by XRF.

Catalyst	Re/Ir molar ratio (nominal)	Composition (wt%)		Re/Ir molar ratio (actual)
		Ir	Re	
20 wt%-Ir Ir/SiO ₂	—	18.0	—	0
ReO _x /SiO ₂	(19.4 wt%) ^a	—	8.4	—
20 wt%-Ir Ir-ReO _x /SiO ₂	0.5	17.7	3.9	0.22
	1	19.8	6.7	0.34
	2	23.7	8.8	0.37
20 wt%-Ir Ir-ReO _x /SiO ₂ ^b	1	19.8	10.8	0.55
4 wt%-Ir Ir-ReO _x /SiO ₂	1	3.9	3.2	0.83
6 wt%-Ir Ir-ReO _x /SiO ₂	1	7.0	4.6	0.65
10 wt%-Ir Ir-ReO _x /SiO ₂	1	10.2	4.9	0.48
30 wt%-Ir Ir-ReO _x /SiO ₂	1	32.0	6.8	0.21
40 wt%-Ir Ir-ReO _x /SiO ₂	1	50.0	6.7	0.13

^a Loading amount of Re.

^b Calcined at 673 K for 3 h. In other cases, catalysts were calcined at 773 K for 3 h.

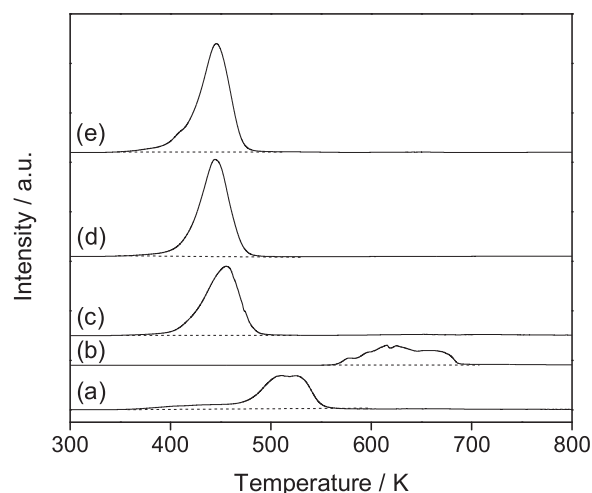


Fig. 2. TPR profiles of (a) 20 wt% Ir/SiO₂, (b) 8.4 wt% ReO_x/SiO₂, (c) 20 wt% Ir-ReO_x/SiO₂, Re/Ir = 0.22, (d) Re/Ir = 0.34, (e) Re/Ir = 0.37 (actual ratio of Re/Ir). Conditions: sample = 30–50 mg, and H₂/Ar (5% v/v, 30 cm³ min⁻¹) at heating rate of 10 K min⁻¹. Y-axis is normalized by the weight of the catalyst. Valence of Re determined by TPR and XRF is shown in Table S3.

3.4. Effect of reduction temperature

Fig. 2 shows the TPR results of 20 wt% Ir/SiO₂, 8.4 wt% ReO_x/SiO₂ and 20 wt%-Ir Ir-ReO_x/SiO₂ (nominal Ir loading amount) with various Re/Ir ratio after calcination at 773 K for 1 h. The Ir/SiO₂ was reduced at the temperature range from 350 to 550 K, and the ReO_x/SiO₂ (8.4 wt% Re, Table 2) showed a wide reduction peak from 550 to 700 K. Similarly to 4 wt%-Ir Ir-ReO_x/SiO₂ [15], only one large peak of H₂ consumption was observed over 20 wt%-Ir Ir-ReO_x/SiO₂ (350–510 K). The reduction temperature was shifted from that of Ir/SiO₂ to lower temperature range, showing the promotion of Ir reduction by Re, similarly to the case of 4 wt%-Ir Ir-ReO_x/SiO₂ [15]. The peak top of reduction temperature of 20 wt%-Ir Ir-ReO_x/SiO₂ (433–455 K) was similar to 4 wt% Ir-ReO_x/SiO₂ (449 K) [15]. The reduction almost completed at 473 K (typical temperature for liquid-phase reduction before use). The amount of consumed H₂ is summarized in Table S3. Based on TPR and XRF data, average valence of Re increased gradually with the increase of Re/Ir ratio. The valence of Re was +2.3 on 20 wt%-Ir Ir-ReO_x/SiO₂ (Re/Ir = 0.34), which was consistent with the Re average valence (+2.7) calculated by XANES and EXAFS analysis as discussed later.

Table 3 lists the reaction results of 20 wt%-Ir Ir-ReO_x/SiO₂ (Re/Ir = 0.34, actual) reduced at different conditions including liquid-phase and gas-phase reductions. In contrast to Re₂O₇, Re oxides with lower

Table 3Glycerol hydrogenolysis over 20 wt%-Ir Ir-ReO_x/SiO₂ (Re/Ir = 0.34, actual) catalyst after various reduction conditions.

Entry	Reduction conditions	time / h	Conv. / %	Selectivity / %				
				1,3-PrD	1,2-PrD	1-PrOH	2-PrOH	Others
1	(L, 473)	4	23	65	5	23	6	1
2	(G, 473)	4	19	60	9	24	4	3
3	(G, 773)	4	18	63	8	23	5	1
4	(G, 973)	4	3	52	21	16	8	2
5	(L, 473)	24	69	47	6	37	9	3
6	(G, 473)	24	75	34	5	48	6	7
7	(G, 773)	24	42	54	9	29	6	2
8	(G, 973)	24	7	46	28	15	9	2

Reaction conditions: 20 wt%-Ir Ir-ReO_x/SiO₂ = 30 mg (Ir amount = 6 mg (31 μmol)), 67 wt% glycerol solution (glycerol = 4 g (43 mmol), H₂O = 2 g), P(H₂) = 8 MPa, T = 393 K. Reduction conditions: 30 cm³ min⁻¹ H₂ at 473, 773 or 973 K for 1 h (gas phase). P(H₂) = 8 MPa at 473 K for 1 h (liquid phase). PrD, propanediol; PrOH, propanol. Others: ethylene glycol + ethanol + propane + methane.

valence are known to rarely sublime [55,56], and we think that the loss of Re in gas-phase reduction is negligible. Ir-ReO_x/SiO₂ catalyst reduced at 473 K demonstrated comparable activity (entries 1–2 and 5–6) regardless of reduction methods. The selectivity of 1,3-PrD was slightly lower over gas-phase reduced catalyst. The increase of reduction temperature above 473 K decreased the activity. The change of product selectivity was difficult to discuss since the conversion level was not the same. Nevertheless, the 1,3-PrD yield was decreased significantly when reduction temperature gradually rose to 973 K. Considering the TPR results (Fig. 2), the activity decrease is not due to the change of reduction degree of catalyst. It can be explained by the aggregation of the Ir metal particles (5.2 nm after reduction at 973 K) in Fig. S4. As a result, liquid-phase reduction at 473 K was selected as the standard method for catalyst pre-reduction.

3.5. Effect of acid addition

In our previous report on 4 wt%-Ir Ir-ReO_x/SiO₂ catalyst, stabilization of the active sites by sulfuric acid addition has been proposed, and the activity is about half of original one without H₂SO₄ addition [15]. Fig. 3 demonstrates the effect of acid addition on initial activity of 4 wt% Ir and 20 wt%-Ir Ir-ReO_x/SiO₂ (Re/Ir = 1, nominal) in 1,2-PrD and glycerol hydrogenolysis. TOF (CO) value was calculated from CO adsorption result which gives 19% and 18% dispersion of surface Ir metal for 4 wt%-Ir and 20 wt%-Ir Ir-ReO_x/SiO₂ (Re/Ir = 1, nominal) as discussed later. For 4 wt%-Ir Ir-ReO_x/SiO₂, higher TOF value was achieved both in glycerol and 1,2-PrD hydrogenolysis when sulfuric acid was added (H⁺/Ir = 1) as previously described [15]. Moreover, the 1,3-PrD selectivity in glycerol hydrogenolysis increased slightly with an addition of H₂SO₄, while 1-PrOH selectivity was unchanged in 1,2-PrD hydrogenolysis. Recent report by means of MD simulations and DFT calculations suggested that the possible promoting effect of H₂SO₄ addition was due to the increasing glycerol concentration within the silica pores and enhancement of the interaction between glycerol and catalyst [57]. However, for 20 wt%-Ir Ir-ReO_x/SiO₂, the addition of H₂SO₄ hardly affected the hydrogenolysis reactions. On the other hand, when HReO₄ was selected to provide H⁺ (H⁺/Ir = 0.5) in the solution, the reaction hardly proceeded over both 4 wt%-Ir and 20 wt%-Ir Ir-ReO_x/SiO₂. This result indicates that the active site is very sensitive to Re species.

In order to clarify the catalyst deactivation when HReO₄ was added, we increased the amount of HReO₄ (H⁺/Ir = 1) for direct comparison with H₂SO₄ addition and measured the change of pH values in glycerol hydrogenolysis. The glycerol conversion was still very low when increasing the HReO₄ amount (Table S4). In blank test without acid addition (Table S4), the solutions mixed with 4 wt%-Ir and 20 wt%-Ir Ir-ReO_x/SiO₂ after reduction were acidic (pH value < 5), which is caused by a small amount of high valence Re species. The acidity decreased slightly in both mixed solutions after reaction. In the case of H₂SO₄

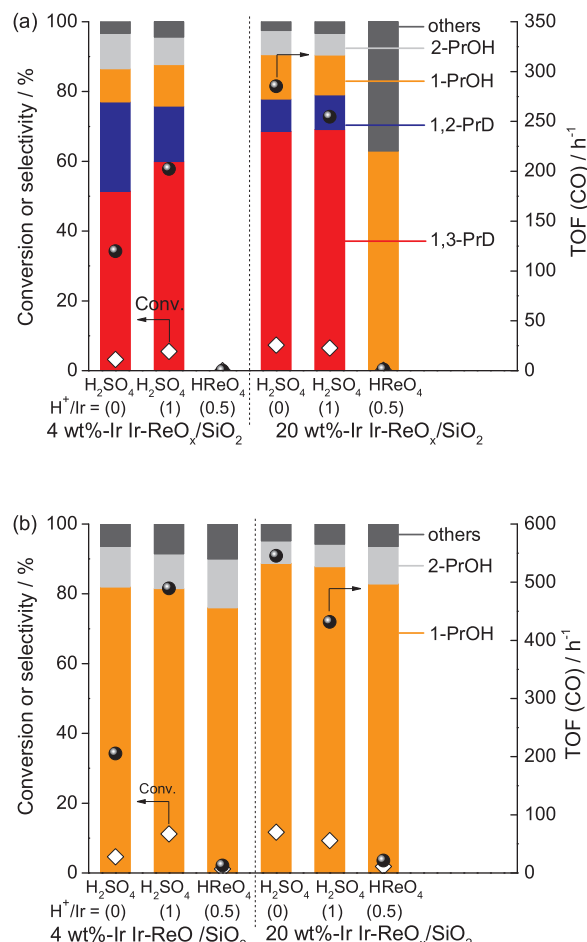


Fig. 3. Effect of acid addition on glycerol (a) and 1,2-PrD (b) hydrogenolysis over 4 wt%-Ir Ir-ReO_x/SiO₂ (Re/Ir = 0.83, actual) and 20 wt%-Ir Ir-ReO_x/SiO₂ (Re/Ir = 0.34, actual) catalyst. Reaction conditions: glycerol or 1,2-PrD = 2 g, H₂O = 38 g, H₂SO₄ = 1.5 mg (H⁺/Ir = 1) or HReO₄ = 3.9 mg (H⁺/Ir = 0.5), P(H₂) = 8 MPa, T = 393 K, t = 1 h, 4 wt%-Ir Ir-ReO_x/SiO₂ = 150 mg, 20 wt%-Ir Ir-ReO_x/SiO₂ = 30 mg (Ir amount = 6 mg (31 μmol)). Reduction conditions: reduction temperature 473 K, reduction time 1 h, H₂ pressure 8 MPa. PrD, propanediol; PrOH, propanol. Others: ethylene glycol + ethanol + propane + ethane + methane. The data as table form are shown in Table S4.

addition, the pH value of solutions was almost unchanged before and after reaction. However, in the case of HReO₄ addition, obvious decrease of acidity of solutions after reaction was observed (Table S4). The increase of pH value after reaction can be explained by the reduction of ReO₄⁻ anion to Reⁿ⁺ species (ReO₄⁻ + H⁺ + H₂ → ReO_x

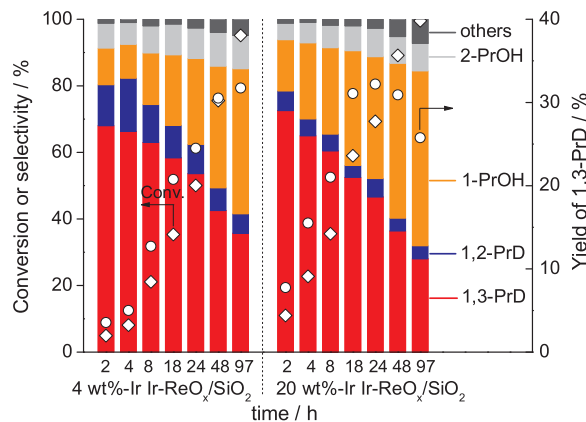


Fig. 4. Time course of the hydrogenolysis of glycerol over 4 wt%–Ir and 20 wt%–Ir $\text{Ir}-\text{ReO}_x/\text{SiO}_2$. Reaction conditions: 67 wt% glycerol solution (glycerol = 4 g (43 mmol), H_2O = 2 g), $P(\text{H}_2)$ = 8 MPa, T = 393 K, 4 wt%–Ir $\text{Ir}-\text{ReO}_x/\text{SiO}_2$ = 150 mg, 20 wt%–Ir $\text{Ir}-\text{ReO}_x/\text{SiO}_2$ = 30 mg (Ir amount = 6 mg (31 μmol)). Reduction conditions: reduction temperature 473 K, reduction time 1 h, H_2 pressure 8 MPa. PrD, propanediol; PrOH, propanol. Others: ethylene glycol + ethanol + propane + ethane + methane. The data as table form are shown in Table S7.

+ H_2O) during the reaction. The 20 wt%–Ir $\text{Ir}-\text{ReO}_x/\text{SiO}_2$ samples with HReO_4 addition ($\text{H}^+/\text{Ir} = 1$) after liquid-phase reduction and reaction were both used for CO adsorption, and the dispersion of Ir metal was only 3% over both catalysts (Table 5, entry 7). This value is much smaller than the 20 wt%–Ir $\text{Ir}-\text{ReO}_x/\text{SiO}_2$ (I, 473) after reduction (Table 5, 18% dispersion of Ir based on CO adsorption), indicating that the high coverage of Re^{n+} species on Ir metal surface will decrease the activity significantly. It is likely that the adsorption of H_2 molecules on Ir metal surface is suppressed, leading to the catalyst deactivation.

3.6. Performance of 20 wt%–Ir $\text{Ir}-\text{ReO}_x/\text{SiO}_2$ catalyst

The time course of the glycerol hydrogenolysis over 4 wt%–Ir $\text{Ir}-\text{ReO}_x/\text{SiO}_2$ ($\text{Re}/\text{Ir} = 0.83$, actual) and 20 wt%–Ir $\text{Ir}-\text{ReO}_x/\text{SiO}_2$ ($\text{Re}/\text{Ir} = 0.34$, actual) without addition of sulfuric acid is shown in Fig. 4. Similar patterns are observed over both catalysts with a difference in activity. The 1,3-PrD selectivity decreased gradually because of the overhydrogenolysis to 1-PrOH, which means that the maximum 1,3-PrD yield will be obtained at an appropriate reaction time. The maximum 1,3-PrD yield was 32% at 1,3-PrD selectivity to 36% at 95% conversion for 97 h over 4 wt%–Ir $\text{Ir}-\text{ReO}_x/\text{SiO}_2$. The highest 1,3-PrD yield over 20 wt%–Ir $\text{Ir}-\text{ReO}_x/\text{SiO}_2$ was also 32%, which obtained at shorter reaction time (24 h) due to the higher activity than 4 wt%–Ir catalyst. The highest $P_{1,3-\text{PrD}}$ was obtained at shorter time over $\text{Ir}-\text{ReO}_x/\text{SiO}_2$ catalytic system because of the high reaction rate and 1,3-PrD selectivity at the initial stage (23% conv. and 65% 1,3-PrD selectivity). The $P_{1,3-\text{PrD}}$ reached $21.5 \text{ g g}_{\text{Ir}}^{-1} \text{ h}^{-1}$ over 20 wt%–Ir $\text{Ir}-\text{ReO}_x/\text{SiO}_2$ for 4 h (initial stage) and $7.4 \text{ g g}_{\text{Ir}}^{-1} \text{ h}^{-1}$ at highest 1,3-PrD yield (32%, 24 h). These values are higher than $17.7 \text{ g g}_{\text{Ir}}^{-1} \text{ h}^{-1}$ for 4 h and $5.8 \text{ g g}_{\text{Ir}}^{-1} \text{ h}^{-1}$ at highest 1,3-PrD yield (38%, 36 h) over 4 wt%–Ir $\text{Ir}-\text{ReO}_x/\text{SiO}_2 + \text{H}_2\text{SO}_4$ system under similar reduction and reaction conditions [13, 15]. These values are comparable to the reported value ($6.8 \text{ g g}_{\text{Ir}}^{-1} \text{ h}^{-1}$, 40% conv. and 37% 1,3-PrD selectivity) over Ir–Re alloy catalyst [58], but higher than the highest value ($5.1 \text{ g g}_{\text{Pt}}^{-1} \text{ h}^{-1}$) among Pt–WO_x based catalysts achieved over Pt–WO_x/t-ZrO₂ at 413 K for 24 h (78% conv. and 63% 1,3-PrD selectivity) in very recent report (Table S5) [28].

The reactivities of various alcohols and hydroxylated ethers over 4 wt%–Ir and 20 wt%–Ir $\text{Ir}-\text{ReO}_x/\text{SiO}_2$ without sulfuric acid addition were compared, and results are listed in Table S6. Similarly to 4 wt%–Ir $\text{Ir}-\text{ReO}_x + \text{H}_2\text{SO}_4$ system [15], the 20 wt%–Ir $\text{Ir}-\text{ReO}_x/\text{SiO}_2$ gave high reactivity of ethylene glycol, 1,2-PrD and glycerol hydrogenolysis with the selective cleavage of internal OH groups when present. $\text{Ir}-\text{ReO}_x/\text{SiO}_2$

catalyst was less reactive in 1,3-PrD hydrogenolysis, which accounted for the high 1,3-PrD selectivity. The $\text{Ir}-\text{ReO}_x/\text{SiO}_2$ was highly active in ethereal C–O hydrogenolysis with –O–C–CH₂OH structure (Table S6, entries 7–12), giving rise to the production of the corresponding primary alcohols. In addition, the position of the OH group (terminal or internal) in hydroxylated ethers can affect the reactivity of the neighboring ether bond (Table S6, entries 15 and 16): lower TOF was obtained in 1-methoxy-2-propanol hydrogenolysis to methanol and 2-propanol. The 20 wt%–Ir $\text{Ir}-\text{ReO}_x/\text{SiO}_2$ ($\text{Re}/\text{Ir} = 0.34$, actual) showed about two-fold higher activity than 4 wt%–Ir $\text{Ir}-\text{ReO}_x/\text{SiO}_2$ ($\text{Re}/\text{Ir} = 0.83$, actual) in hydrogenolysis of all the substrates screened. These selectivity patterns are in accordance with the 4 wt%–Ir $\text{Ir}-\text{ReO}_x/\text{SiO}_2 + \text{H}_2\text{SO}_4$ system, supporting the direct hydrogenolysis mechanism of C–O bond neighboring to the terminal –CH₂OH group proposed in previous work [13, 15, 34].

Then we examined the reusability of 4 wt%–Ir ($\text{Re}/\text{Ir} = 0.83$, actual) and 20 wt%–Ir $\text{Ir}-\text{ReO}_x/\text{SiO}_2$ ($\text{Re}/\text{Ir} = 0.34$, actual). First, the used catalyst was recovered, dried and calcined in air before next use [15]. These data are summarized in Fig. S5. The activity of 20 wt%–Ir $\text{Ir}-\text{ReO}_x/\text{SiO}_2$ after three times of usage was significantly decreased, and the glycerol conversion is comparable to that over fresh 4 wt%–Ir $\text{Ir}-\text{ReO}_x/\text{SiO}_2$. Additionally, the performance of 4 wt%–Ir $\text{Ir}-\text{ReO}_x/\text{SiO}_2$ cannot be recovered even compensated with fresh catalyst as our previous report [15] where good reusability of 4 wt%–Ir $\text{Ir}-\text{ReO}_x/\text{SiO}_2$ was obtained with addition of H_2SO_4 . The Ir and Re leaching amount of 20 wt%–Ir $\text{Ir}-\text{ReO}_x/\text{SiO}_2$ ($\text{Re}/\text{Ir} = 0.34$, actual) were investigated using ICP-AES. We measured the leaching amount after each reaction in the three times of reuse under reaction conditions (b) of Fig. S5. Significantly, the leaching amount of both Ir and Re after each batch was very small (Ir: < 0.1% and Re: < 0.25%, based on actual loading amount of Ir and Re). If one compares these data to 2% for Ir and 0.9% for Re over 4 wt%–Ir $\text{Ir}-\text{ReO}_x/\text{SiO}_2$ ($\text{Re}/\text{Ir} = 1$, nominal) [15], < 0.3% for both Ir and Re in the presence of H_2SO_4 using 4 wt%–Ir $\text{Ir}-\text{ReO}_x/\text{SiO}_2$ ($\text{Re}/\text{Ir} = 1$, nominal) [13], and 0.5% for Ir and 0.4% for Re in the presence of HZSM-5 after one-batch glycerol hydrogenolysis [33], although the reaction conditions were different, it can be concluded that the high loading amount of $\text{Ir}-\text{ReO}_x$ pairs favors the stabilization of active site on catalyst surface. Due to the very small leaching amount for 20 wt%–Ir $\text{Ir}-\text{ReO}_x/\text{SiO}_2$ after catalytic use, one possible interpretation of the deactivation is the effect of the Re^{n+} species desorbed by oxidation and redorsed on the Ir metal surface over catalyst, considering that addition of HReO_4 to $\text{Ir}-\text{ReO}_x/\text{SiO}_2$ much decreased the activity (Fig. 3). In the reuse test, catalyst was exposed to air with a small amount of water during the recovery. Some amount of Re species was oxidized to ReO_4^- anion as it is the only Re species that has high solubility in water [23, 59]. The ReO_4^- anion could be partially reduced to Re^{n+} species at high H_2 pressure during the reduction and reaction (8 MPa H_2). Therefore, the Re^{n+} species tend to strongly interact with Ir metal surface, affecting the stability of active site. The Ir particle size after four times reuse was still very small (3.2 nm, Fig. S4).

Then another method was attempted where the catalyst was not exposed to air to improve the reusability of 20 wt%–Ir $\text{Ir}-\text{ReO}_x/\text{SiO}_2$. The scale of the reaction was doubled (2 g glycerol, 18 g H_2O and 60 mg catalyst) to decrease the amount of catalyst loss during the reuse process. It was confirmed that the scale-up does not affect the performance (Fig. S5, first use of 20 wt%–Ir $\text{Ir}-\text{ReO}_x/\text{SiO}_2$ under reaction conditions of (a) and (b)). Because the catalyst was obtained in wet form, the accurate amount of the catalyst after reaction cannot be determined in each test. We measured the catalyst amount after four times reuse, and it was 29 mg, representing for about 20 wt% loss of catalyst after each reuse test. The amount of glycerol and water solvent was adjusted to keep glycerol/water/catalyst weight ratio 1/9/0.03. Both the conversion rate and 1,3-PrD selectivity were almost constant for the reusability tests (Table 4), indicating the catalyst can be reused at least three times without activity and selectivity decrease.

Table 4Reusability of 20 wt% Ir Ir-ReO_x/SiO₂ (Re/Ir = 0.34, actual) without exposure to air after reaction.

Glycerol amount / g	H ₂ O amount / g	Catalyst amount / mg	Usage times	Conv. / %	Selectivity / %					Conversion rate / mmol.g-Cat ⁻¹ .h ⁻¹
					1,3-PrD	1,2-PrD	1-PrOH	2-PrOH	Others	
2.0	18.0	60	1	38	58	7	25	8	2	69.4
1.6	14.5	(47) ^a	2	35	61	8	21	8	2	65.3
1.3	11.6	(37) ^a	3	34	62	10	18	8	2	66.0
1.0	9.0	29	4	38	61	11	18	8	2	69.9

Reaction conditions: $P(H_2) = 8 \text{ MPa}$, $T = 393 \text{ K}$, $t = 2 \text{ h}$. The initial amount of glycerol and H₂O was 2 g and 18 g, respectively. The catalyst was directly reused without exposure to air.

^a estimated amount from the final catalyst amount.

3.7. Catalyst characterization

XRD results of catalysts with various Ir loading amount after the catalytic use and exposure to air are demonstrated in Fig. 5. XRD patterns of monometallic Ir/SiO₂ after liquid-phase reduction (L, 473) and other related catalysts after reduction or reaction are also shown in Fig. S6. The peaks at about $2\theta = 41, 47, 69^\circ$ are assigned to Ir metal [60], which was in accordance with 4 wt% Ir Ir-ReO_x/SiO₂ with H₂SO₄ addition after reaction [15]. The average metal size of Ir was very small, ranging from 2.5 to 3.7 nm when Ir loading amount was between 4 wt %-Ir and 40 wt%-Ir (nominal). The average particle size which was counted by TEM images agreed well with that calculated from the linewidth of the XRD peak (Figs. 5 and 6 and S7). Additionally, small peaks at 37.8, 40.6 and 42.6° assigned to Re metal with hexagonal closed packed structure (Re(HCP)) were detected when Ir amount was in the range between 4 wt%-Ir and 8 wt%-Ir. However, this peak was not observed at higher loading of Ir-ReO_x pairs, indicating most Re species are highly dispersed or non-crystalline. The EDX analysis was also carried out for 20 wt% Ir Ir-ReO_x/SiO₂ (Re/Ir = 0.34, actual, Fig. S8). However, little information for Re dispersion was obtained probably because of the oxidation of Re by air before measurement.

Table 5 lists the CO adsorption amount on reduced catalysts to determine the dispersion of Ir metal on the catalyst surface. We previously reported that the ReO_x/SiO₂ cannot adsorb CO molecule [15], and therefore CO adsorption amount represents for the surface Ir metal atoms. The CO adsorption amount for Ir-ReO_x/SiO₂ catalysts was similar to corresponding monometallic Ir/SiO₂. Another aspect was that the Ir particle size of catalysts with Re addition was significantly smaller than the corresponding monometallic Ir/SiO₂. These data suggest the Ir metal was partially covered with Re species, which has been explained by Rh-ReO_x/SiO₂ [14] and 4 wt% Ir Ir-ReO_x/SiO₂ [15]. Moreover, the Ir/SiO₂ and Ir-ReO_x/SiO₂ reduced in liquid phase or gas

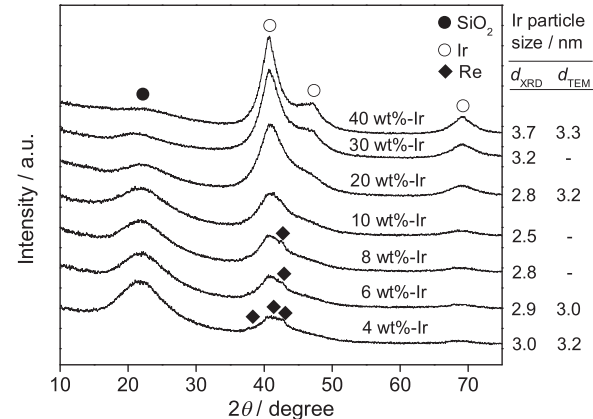


Fig. 5. XRD patterns of the Ir-ReO_x/SiO₂ with Ir loading amount varied from 4 wt% to 40 wt% after liquid-phase reduction at 473 K and the catalytic use at standard reaction conditions.

phase at 473 K showed almost the same dispersion based on CO adsorption (Table 5, entries 3–6).

FT-IR and XRD measurements without exposure to air were conducted to further examine the oxidized state of Re over catalyst (20 wt% Ir, Re/Ir = 0.34, actual). The adsorbed CO on the reduced catalysts was clearly observed as one single band in the FT-IR spectra as shown in Fig. S9. The position of the peak was 2067, 2065 and 2067 cm⁻¹ for 20 wt% Ir/SiO₂, 4 wt%-Ir and 20 wt%-Ir Ir-ReO_x/SiO₂, respectively. This peak is ascribed to the linearly adsorbed CO on the Ir metal. If metallic Re species is exposed on the catalyst surface, the adsorption band should be broadened because of the lower wavenumber of CO adsorption on Re⁰ (2030–2050 cm⁻¹) [61–64]. However, the signal pattern was very similar between 20 wt%-Ir Ir-ReO_x/SiO₂ and 20 wt% Ir/SiO₂,

Table 5Summary of characterization results of Ir/SiO₂ and Ir-ReO_x/SiO₂ (Re/Ir = 1, nominal).

Entry	Catalyst	Ir size / nm		Dispersion / %		Valence of Re	
		XRD	TEM	CO adsorption	XRD	TPR ^c	XANES
1	4 wt% Ir/SiO ₂ (L, 473)	3.7	–	16	30	–	–
2	4 wt%-Ir Ir-ReO _x /SiO ₂ (L, 473)	3.0	3.2	19	37	3.6 ^d	2.8 ^d
3	20 wt% Ir/SiO ₂ (G, 473)	–	–	15	–	–	–
4 ^a	20 wt% Ir/SiO ₂ (L, 473)	3.5	–	16	31	–	–
5	20 wt%-Ir Ir-ReO _x /SiO ₂ (G, 473)	3.2	–	18	34	2.3	2.7
6 ^a	20 wt%-Ir Ir-ReO _x /SiO ₂ (L, 473)	2.8	3.2	18	39	–	1.1
7 ^b	20 wt%-Ir Ir-ReO _x /SiO ₂ (L, 473) + HReO ₄	–	–	3	–	–	–

^a Liquid-phase reduction at $P(H_2) = 8 \text{ MPa}$ and $T = 473 \text{ K}$ for 1 h before CO adsorption.

^b Catalyst was obtained after liquid-phase reduction (L, 473) and catalytic use (reaction conditions: glycerol = 0 g or 2 g (22 mmol), H₂O = 38 g, HReO₄ = 7.8 mg (H⁺/Ir = 1), $P(H_2) = 8 \text{ MPa}$, $T = 393 \text{ K}$, $t = 1 \text{ h}$, 20 wt%-Ir Ir-ReO_x/SiO₂ = 30 mg (Ir amount = 6 mg (31 μmol)). In other cases, catalyst was reduced by H₂ flow at 473 K for 1 h.

^c $7.2 \times [\text{amount of H}_2 \text{ consumed, } \mu\text{mol}] - 2 \times [\text{actual Ir loading amount, } \mu\text{mol}]/[\text{actual Re loading amount, } \mu\text{mol}]$. The 4 wt% and 20 wt% Ir/SiO₂ catalysts were reduced without activity test. In other cases, XRD data were obtained from the catalysts after reduction and the catalytic use.

^d Ref. [15].

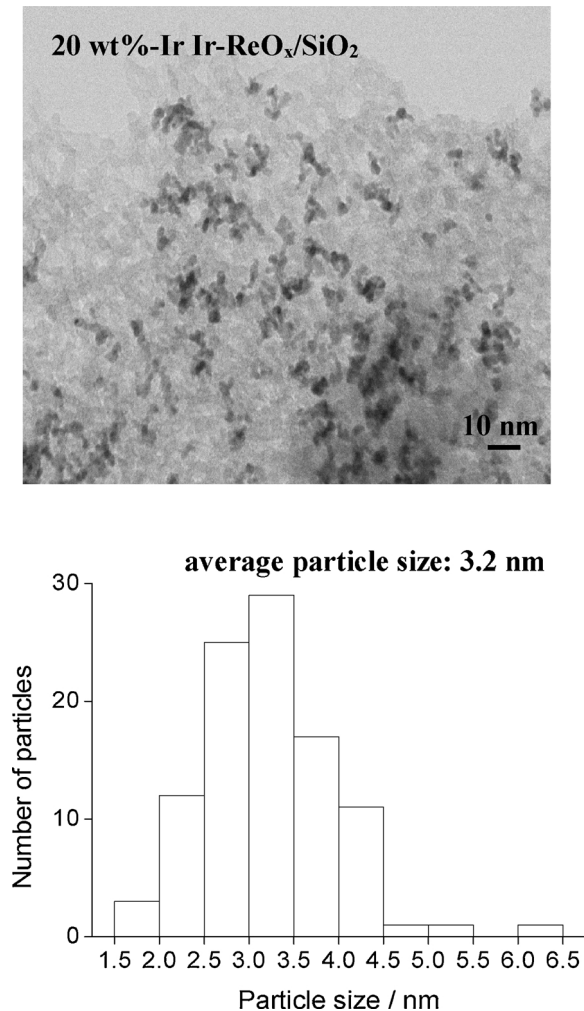


Fig. 6. TEM image of 20 wt%–Ir–ReO_x/SiO₂ (Re/Ir = 0.34, actual) catalyst after liquid-phase reduction at 473 K and the catalytic use at standard reaction conditions.

suggesting the absence of Re metal species on the very surface. The XRD result without exposure to air (Fig. S10) also supports the absence of Ir–Re alloy phase since no obvious shift of diffraction peak on Ir metal was observed. The small peaks assigned to Re (HCP) were also detected only over 4 wt%–Ir–ReO_x/SiO₂ after reaction. These peaks of Re (HCP) were not observed over 4 wt%–Ir and 20 wt%–Ir–ReO_x/SiO₂ after gas-phase reduction or after gas-phase reduction and reaction (Fig. S6).

The Ir L₃-XANES spectra were examined, and the results for catalysts after gas-phase reduction (G, 473) and catalyst after liquid-phase reduction (L, 473) and catalytic use are shown in Fig. S11. The 20 wt% Ir/SiO₂ and 20 wt%–Ir–ReO_x/SiO₂ (Re/Ir = 0.34, actual) catalysts after reduction or reaction showed similar spectra to Ir metal powder. It suggests that the Ir species are fully reduced to metallic state (IrO₂ + 2H₂ → Ir + 2H₂O). For calcined catalyst, the spectrum was similar to that of IrO₂. The results of Ir L₃-edge EXAFS analysis are presented in Table 6 and Fig. S12. The presence of Ir–Ir (or -Re) bond with bond distance of 0.275 nm and coordination number (CN) of 10.5–11.2 over Ir/SiO₂, 20 wt%–Ir–ReO_x/SiO₂ (G, 473) and 20 wt%–Ir–ReO_x/SiO₂ (L, 473) after reaction (Table 6, entries 1–3) is shown by the curve fitting results. The Ir metal phase is also supported by XRD, indicating the Ir species over 20 wt%–Ir–ReO_x/SiO₂ are in metallic state in regardless of the reduction method at 473 K. This result is similar to the 4 wt%–Ir–ReO_x/SiO₂ (Re/Ir = 0.83, actual) + H₂SO₄ after reaction (Table 6, entry 4) [15].

The Re L₃-XANES spectra of catalysts reduced by different methods

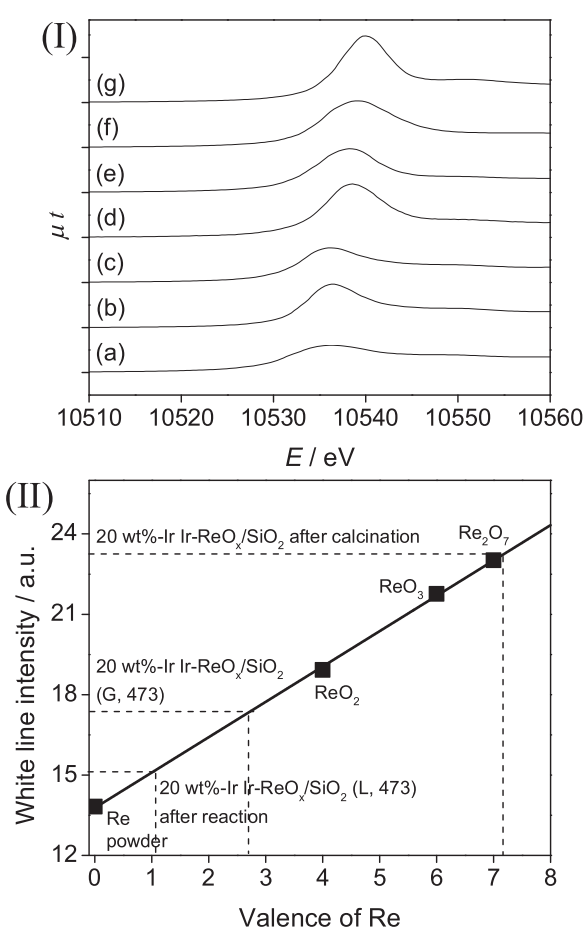
and reference compounds are presented in Fig. 7. The average valence of Re was calculated by our previously reported method using white line intensity [14,15,52,65]. It was determined to be +2.7 and +1.1 (Table 5, entries 5 and 6), on gas-phase reduced catalyst (G, 473) and on liquid-phase reduced catalyst (L, 473) after use, respectively. Same Re valence (+7) was obtained over calcined catalyst (20 wt% Ir, Re/Ir = 0.34, actual) and the Re precursor (NH₄ReO₄). According to our previous reports, Re species over Ir–ReO_x/SiO₂ (4 wt% Ir, Re/Ir = 1, nominal), Rh–ReO_x/SiO₂ (4 wt% Rh, Re/Rh = 0.5, nominal) and Pt–ReO_x/SiO₂ (2 wt% Pt, Re/Pt = 0.5, nominal) reduced at corresponding optimized conditions shows a similar valence of +3, +2 and +2/+3, respectively [14,15,65]. The higher reduction degree of Re species on 20 wt%–Ir–ReO_x/SiO₂ after reaction can be interpreted by the high Re loading amount. It has been found that Re species on 14 wt% Re/SiO₂ (nominal) was prone to be reduced to lower valence conditions [52].

We further examined the Re L₃-edge EXAFS spectra of catalyst after gas-phase reduction (G, 473) and catalyst after liquid-phase reduction (L, 473) and use in glycerol hydrogenolysis. The curve fitting results are summarized in Table 7, and the raw spectra are shown in Fig. S13. The Re–O bond with bond distance of 0.213–0.214 nm was slightly longer than that over 4 wt%–Ir–ReO_x/SiO₂ (0.202–0.203 nm) [15] and Pt–ReO_x/SiO₂ (0.204–0.205 nm) [66], and similar to Rh–ReO_x/SiO₂ (0.210–0.213 nm) [67]. The presence of Re–O bond suggests the presence of ReO_x species, which is in agreement with Re L₃-edge XANES and TPR results. Moreover, the Re–Ir (or -Re) bond distance was 0.268 nm (Table 7), which was shorter than Ir–Ir (or -Re) bond (0.275 nm, Table 6, entry 2). The difference of bond distance between Re–Ir (or -Re) and Ir–Ir (or -Re) in Re and Ir EXAFS, respectively, suggests that Ir–Re alloy was not formed. Furthermore, CN of Re–Re (or -Ir) over 20 wt%–Ir–ReO_x/SiO₂ (G, 473) and 20 wt%–Ir–ReO_x/SiO₂ (L, 473) after reaction was evidently higher than that over 4 wt%–Ir–ReO_x/SiO₂ (L, 473) + H₂SO₄ after reaction (Table 7). It should be pointed out that the CN of Re–Re (or -Ir) (10.2) over catalyst reduced in gas phase is higher than that of 20 wt%–Ir–ReO_x/SiO₂ (L, 473) after reaction (8.6), while the average valence of Re (+2.7) after gas-phase reduction is higher than that of used catalyst (+1.1). Considering the similar dispersion determined from XRD and CO adsorption (Table 5, entries 5 and 6), one possible explanation is that the Re species over gas-phase reduced catalyst formed larger particles than 20 wt%–Ir–ReO_x/SiO₂ (L, 473) after reaction in a local region. This increase of CN_{Re-Re} was also found over Pt–Re/C after thermal treatment, leading to the formation larger Re particles with higher CN_{Re-Re} (6→10) [68].

According to literature, the water molecules can be activated on Re metal [69], Re⁰ atoms on the surface of metallic Pt and Rh [70,71], and ReO_x species over Pt–ReO_x/TiO₂ [72]. For bimetallic Rh/Re/C catalyst [71], the CN of Re–Rh + Re–Re was increased from 6.0 to 8.2 based on EXAFS measurement when the reduction temperature was raised from 393 to 723 K. The Re species with high coordination number decreased the activity in C–O hydrogenolysis because that with low coordination number was responsible for water activation [71]. On the contrary, high CN_{Re-Re} (or -Ir) on the 20 wt%–Ir–ReO_x/SiO₂ after reaction were observed in this study. It suggests that the water activation mode was not the same between the Re sites on the surface of Rh and low valence ReO_x cluster attached to Ir metal. We think that the water molecules are activated and converted into Re–OH site, rather than working as acid on the surface of the low valence Re species attached to Ir metal over this catalyst during the reduction pretreatment and reaction. Since the 20 wt%–Ir–ReO_x (Re/Ir = 0.34, actual) after liquid-phase reduction (L, 473) can be reused, a model structure of 20 wt%–Ir–ReO_x during reaction is proposed in view of the characterization results (Fig. 8). The 4 wt%–Ir–ReO_x/SiO₂ (Re/Ir = 0.83, actual) after reduction at 485–595 K in H₂ flow demonstrated three-dimensional ReO_x clusters (average valence: ~+3) attached to the cuboctahedral Ir metal particles (~2 nm), which gave the CN_{Re-Re} (or -Ir) about 6.0–6.5 [36]. Another important point is that the Ir particle size (XRD) and coverage ratio ($D_{\text{XRD}} - D_{\text{CO}}$) on 4 wt%–Ir and 20 wt%–Ir–ReO_x/SiO₂ are comparable

Table 6Curve fitting results of Ir L_3 -edge EXAFS of Ir-ReO_x/SiO₂ (Re/Ir = 1, nominal) and 20 wt% Ir/SiO₂ after reaction.

Entry	Catalyst	Shells	CN ^a	$R / 10^{-1} \text{ nm}^b$	$\sigma / 10^{-1} \text{ nm}^c$	$\Delta E_0 / \text{eV}^d$	$R_f / \%^e$
1	20 wt%-Ir Ir/SiO ₂ (L, 473) after reaction	Ir-Ir	11.2 ± 0.7	2.75 ± 0.01	0.060 ± 0.003	-1.7 ± 1.5	1.1
2	Ir-ReO _x /SiO ₂ (G, 473) ^f	Ir-Ir (or -Re)	10.8 ± 0.8	2.75 ± 0.01	0.061 ± 0.004	-1.2 ± 1.2	1.0
3	Ir-ReO _x /SiO ₂ (L, 473) ^f after reaction	Ir-Ir (or -Re)	10.5 ± 1.0	2.75 ± 0.01	0.066 ± 0.004	-2.0 ± 1.3	1.2
4	Ir-ReO _x /SiO ₂ (L, 473) ^g after reaction	Ir-Ir (or -Re)	10.5 ± 0.9	2.76 ± 0.01	0.066 ± 0.004	-1.1 ± 1.2	0.9
5	Ir metal	Ir-Ir	12.0	2.77	0.060	0.0	—

^a Coordination number.^b Bond distance.^c Debye-Waller factor.^d Difference in the origin of photoelectron energy between the reference and the sample.^e Residual factor.^f Ir: 20 wt%, Re/Ir = 0.34 (actual).^g Ir: 4 wt%, Re/Ir = 0.83 (actual), Ref. [15]. Fourier filtering range: 0.157–0.325 nm.**Fig. 7.** Results of Re L_3 -edge XANES analysis of 20 wt%-Ir Ir-ReO_x/SiO₂ (Re/Ir = 0.34, actual). (I) Re L_3 -edge XANES spectra. (II) Relation between white line area and valence of Re. (a) Re powder, (b) 20 wt%-Ir Ir-ReO_x/SiO₂ (G, 473), (c) 20 wt%-Ir Ir-ReO_x/SiO₂ after liquid-phase reduction (L, 473) and catalytic use, (d) 20 wt%-Ir Ir-ReO_x/SiO₂ after calcination, (e) ReO₂, (f) ReO₃, (g) Re₂O₇.

(Table 5, entries 2 and 6). The local structure is plausible to be the metallic Ir (~3 nm) with cuboctahedron structure covered with low valence ReO_x clusters (average valence: +1~+2). The accurate location of Re species on Ir surface is difficult to deduce, since relatively high CN_{Re-Re} (or -Ir) (8.6) over catalyst after reaction was obtained from curve fitting result, and no Ir-Re alloy (XRD and EXAFS analysis) or Re metal phase (XRD and CO-FTIR) was observed. The most likely interpretation is that multiple layers of Re species are directly contacted between Ir particles which are densely located on SiO₂ support (Fig. 8). In a local region, Re metal is covered with ReO_x clusters to give high CN_{Re-Re} (or

-Ir) and to suppress the adsorption of CO molecule. The coverage of Re on Ir surface (Ir_s) is calculated from the dispersion (Ir_s/Ir = 0.39, Table 5) and actual Re/Ir ratio (0.34), and it is estimated to be Re/Ir_s ≈ 0.9. Considering the value of Re/Ir_s and available site for CO adsorption, three-dimensional ReO_x clusters attach to Ir metal surface, slightly decreasing the average CN_{Re-Re} (or -Ir). This structure is supported by the condensed Ir particles on silica support (TEM-EDX analysis of Ir, Fig. S8). On the basis of activity and characterization data, we propose that the active site is the Ir-ReO_x interface site mainly located at the edge or corner of Ir particles. The presence of ReO_x clusters located between condensed Ir particles decreases the effect of SiO₂ support (high loading amount, 20 wt%-Ir) because some of Ir particles can be present above the SiO₂ support. In addition, attaching the ReO_x cluster to neighboring two (or more) Ir particles increases the number of Ir-ReO_x interface per Re amount, and thus the number of active site is increased even at lower Re/Ir ratio.

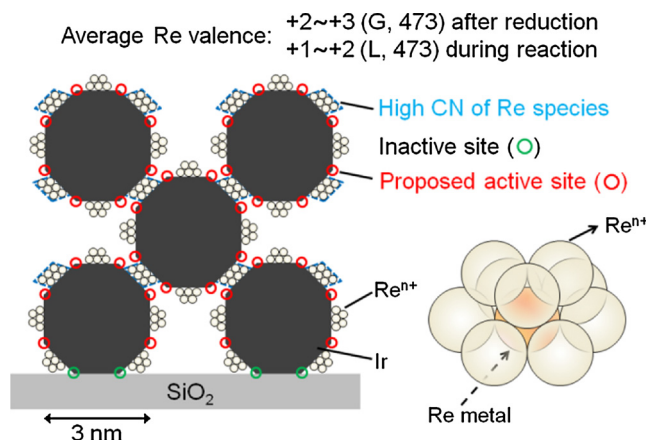
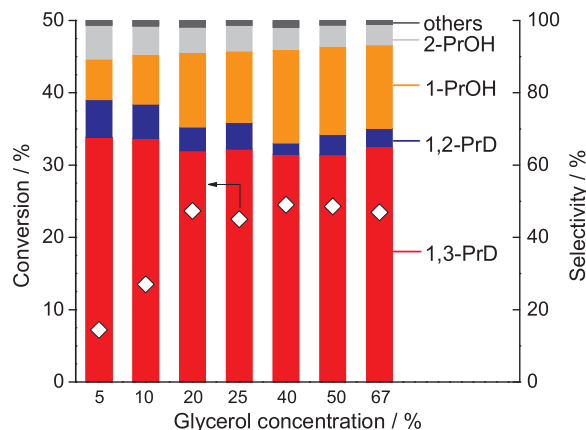
3.8. Kinetics and reaction mechanism

The effect of the H₂ pressure and glycerol concentration on the hydrogenolysis reaction was investigated using 20 wt%-Ir Ir-ReO_x/SiO₂ (Re/Ir = 0.34, actual) catalyst. A well linear relationship between glycerol conversion and H₂ pressure (2–8 MPa) was found over this catalyst (Fig. S14), which gives the reaction order of H₂ about 1. The selectivity of products is independent of H₂ pressure. Similar reaction order (~1) on H₂ pressure under same reaction conditions over 4 wt%-Ir Ir-ReO_x/SiO₂ + H₂SO₄ system has been reported [15]. It suggests that the heterolytic dissociation of H₂ to produce one active hydrogen species [15].

Fig. 9 presents the substrate concentration effect for glycerol hydrogenolysis. The glycerol to Ir amount ratio was set constant (glycerol/Ir = 1.4×10^3 mol/mol), and glycerol concentration was adjusted by changing the H₂O amount. The glycerol conversion, which represents the activity, increased at glycerol concentration in the range of 5–20 wt %, and then it was saturated when the glycerol concentration exceeded 20 wt%. Hence, almost all the glycerol molecules are strongly adsorbed on active sites under standard reaction conditions (67 wt% glycerol), and the reaction order on glycerol concentration around standard reaction conditions is about 0 (Fig. S15). This saturation tendency in high concentration has been also observed over Rh-ReO_x/SiO₂ in 1,2-PrD hydrogenolysis [73] and 4 wt%-Ir Ir-ReO_x/SiO₂ + H₂SO₄ catalytic system in glycerol hydrogenolysis [15]. More importantly, the 1,3-PrD selectivity was almost unchanged at different glycerol concentrations as discussed earlier. This result is in contrast to using 4 wt%-Ir ReO_x/SiO₂ + H₂SO₄ catalytic system where the 1,3-PrD selectivity increased within a glycerol concentration range of 5 wt% to 40 wt% [15]. We also proposed that increasing 1,3-PrD selectivity at higher glycerol concentration is ascribed to higher coverage of 2,3-dihydroxypropoxide which is the precursor of 1,3-PrD via the 1-position adsorption of

Table 7Curve fitting results of Re L_3 -edge EXAFS of Ir-ReO_x/SiO₂ (G, 473, Re/Ir = 1, nominal) and Ir-ReO_x/SiO₂ (L, 473, Re/Ir = 1, nominal) after reaction.

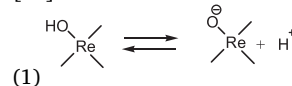
Entry	Catalyst	Shells	CN ^a	R / 10 ⁻¹ nm ^b	σ / 10 ⁻¹ nm ^c	ΔE_0 / eV ^d	R _f / % ^e
1	Ir-ReO _x /SiO ₂ (G, 473) ^f	Re-O	1.2 ± 0.8	2.13 ± 0.04	0.075 ± 0.025	8.1 ± 3.9	1.1
		Re-Re (or -Ir)	10.2 ± 0.8	2.68 ± 0.01	0.052 ± 0.004	-3.3 ± 1.5	
2	Ir-ReO _x /SiO ₂ (L, 473) ^f after reaction	Re-O	0.8 ± 0.6	2.14 ± 0.06	0.060 ± 0.010	4.6 ± 7.5	1.8
		Re-Re (or -Ir)	8.6 ± 1.0	2.68 ± 0.01	0.060 ± 0.006	-3.1 ± 1.4	
3	Ir-ReO _x /SiO ₂ (L, 473) ^g after reaction	Re-O	1.4 ± 0.5	2.02 ± 0.03	0.074 ± 0.021	-0.1 ± 6.5	2.0
		Re-Re (or -Ir)	6.2 ± 0.9	2.68 ± 0.01	0.076 ± 0.008	8.7 ± 2.0	
4	Re metal	Re-Re	12.0	2.74	0.060	0.0	-

^a Coordination number.^b Bond distance.^c Debye-Waller factor.^d Difference in the origin of photoelectron energy between the reference and the sample.^e Residual factor.^f Ir: 20 wt%, Re/Ir = 0.34 (actual).^g Ir: 4 wt%, Re/Ir = 0.83 (actual), Ref. [15]. Fourier filtering range: 0.156–0.331 nm.**Fig. 8.** Model structure of 20 wt% Ir-ReO_x/SiO₂ (Re/Ir = 0.34, actual) during reaction.**Fig. 9.** Effect of glycerol concentration on glycerol hydrogenolysis over 20 wt% Ir-ReO_x/SiO₂ (Re/Ir = 0.34, actual) catalyst with fixed glycerol/catalyst amount ratio. Reaction conditions: glycerol = 4 g, H₂O = 2–16 g, P(H₂) = 8 MPa, T = 393 K, t = 4 h, 20 wt% Ir-ReO_x/SiO₂ = 30 mg. The 5 wt% and 10 wt% of glycerol solutions were adjusted by glycerol = 1 g, H₂O = 19 g, catalyst = 7.5 mg, and glycerol = 2 g, H₂O = 18 g, catalyst = 15 mg, respectively. Reduction conditions: reduction temperature 473 K, reduction time 1 h, H₂ pressure 8 MPa. PrD, propanediol; PrOH, propanol. Others: ethylene glycol + ethanol + propane + ethane + methane.

glycerol on the Re species. Considering the comparable activity of catalysts in these two systems when the conditions are optimized including the addition of acid, the mechanism including the intermediate

structure is the same. The effect of glycerol concentration on 1,3-PrD selectivity is negligible over 20 wt% Ir-ReO_x/SiO₂. High coverage of 2,3-dihydroxypropoxide is formed on 20 wt% Ir-ReO_x/SiO₂ even at lower glycerol concentration.

Overall, the reaction mechanism over 20 wt% Ir-ReO_x/SiO₂ without H₂SO₄ addition is essentially the same to the previously proposed one over 4 wt% Ir-ReO_x/SiO₂ + H₂SO₄ with very slight difference in adsorption of substrate under low substrate concentration. Adsorption of substrates with –CH₂OH group proceeded on ReO_x cluster surface to form terminal alkoxide. Afterwards, hydride derived from heterolytic dissociation of hydrogen molecule on the Ir metal surface attacks the alkoxide at 2-position for the cleavage of C–O bond, and finally releases the product by hydrolysis of the reduced alkoxide [15]. For glycerol hydrogenolysis over 4 wt% Ir-ReO_x/SiO₂, sulfuric acid addition promotes the formation of hydroxorhenium site to increase the total number of adsorbed substrate molecule (Eq. (1)) [33].



The Re–OH site is more stable over this catalyst with higher loading amount since the reaction rate in glycerol and 1,2-PrD hydrogenolysis is almost unchanged when sulfuric acid was added. It can be explained by the decrease of acidity by lower valence of ReO_x clusters attached to Ir metal over high loading amount of Ir-ReO_x pairs (Scheme 1). Therefore, the activity of all substrates is much enhanced over 20 wt% Ir-ReO_x/SiO₂.

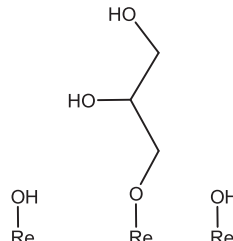
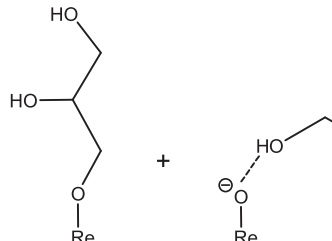
In our previous report [33], we explained that the 1,2-PrD by-product is derived from the glycerol adsorption at 2-position over Ir-ReO_x/SiO₂ catalyst, and this adsorption mode is promoted by surface deprotonated Re-O species, although glycerol adsorption at 1-position as terminal alkoxide is still the dominant adsorbed species [57]. The high 1,3-PrD selectivity even at low glycerol concentration can be ascribed to the high surface concentration of Re–OH above Re–O[−] (Scheme 2) over 20 wt% Ir-ReO_x/SiO₂.

4. Conclusions

The Ir-ReO_x/SiO₂ (Re/Ir = 0.34, actual) catalyst with higher Ir loading amount (20 wt%) and lower ratio of Re/Ir has two-fold higher activity than Ir-ReO_x/SiO₂ (4 wt% Ir, Re/Ir = 0.83, actual), and comparable activity to 4 wt% Ir-ReO_x/SiO₂ + H₂SO₄ in previous report, maintaining high 1,3-propanediol (1,3-PrD) selectivity. The maximum 1,3-PrD yield is 32% with 47% selectivity at 69% conversion at 8 MPa H₂ and 393 K for 24 h. The 1,3-PrD productivity was 21.5 g g_{Ir}⁻¹ h⁻¹ over 20 wt% Ir-ReO_x/SiO₂, which is higher than the 4 wt% Ir-ReO_x/SiO₂ + H₂SO₄ system (17.7 g g_{Ir}⁻¹ h⁻¹) at same reduction and reaction conditions. Loss of Re occurs in samples with higher loading



Scheme 1. Reversible process of protonation of oxorhenium site to hydroxorhenium site.



Scheme 2 Adsorption mode on 4 wt%‐Ir and 20 wt%‐Ir Ir‐BeO_x/SiO₂ catalyst

amount of Re on SiO₂ support during calcination. In regardless of glycerol concentrations, higher 1,3-PrD selectivity was obtained over 20 wt%-Ir Ir-ReO_x/SiO₂, while 4 wt%-Ir Ir-ReO_x/SiO₂ catalyst requires high glycerol concentrations to achieve comparable selectivity. The reactivity of various substrates and kinetics results are similar between this catalyst and previous 4 wt%-Ir Ir-ReO_x/SiO₂ catalyst + H₂SO₄. The catalyst is reusable when this catalyst is recovered without exposure to air.

The Ir metal average particle size almost unchanged by the increase of Ir loading on SiO_2 support. The average Re valence over the catalyst was determined to be about +1~+2 by liquid-phase reduction and catalytic use. Higher reduction degree of Re species on 20 wt%‐Ir $\text{Ir}-\text{ReO}_x/\text{SiO}_2$ after reaction than 4 wt%‐Ir catalyst was observed, and the low valence of ReO_x cluster attached to Ir metal can be stabilized by being located between condensed Ir particles. This structure plays an important role to decrease the effect of SiO_2 support and probably to form the Re‐OH site for substrate adsorption.

Acknowledgements

This work was partially supported by JSPS KAKENHI18H05247. Lujie Liu acknowledges financial support from the China Scholarship Council (CSC). We also appreciate the assistance of TEM measurements by the Technical Division in the School of Engineering in Tohoku University.

Appendix A. Supplementary data

Supplementary material related to this article can be found, in the online version, at doi:<https://doi.org/10.1016/j.apcatb.2019.117775>.

References

- [1] M. Pagliaro, R. Ciriminna, H. Kimura, M. Rossi, C. Della Pina, *Angew. Chem. Int. Ed.* **46** (2007) 4434–4440.

[2] M. Besson, P. Gallezot, C. Pinel, *Chem. Rev.* **114** (2014) 1827–1870.

[3] B. Katryniok, H. Kimura, E. Skrzynska, J.S. Girardon, P. Fongarland, M. Capron, R. Ducoulombier, N. Mimura, S. Paul, F. Dumeignil, *Green Chem.* **13** (2011) 1960–1979.

[4] B. Katryniok, S. Paul, V. Belliere-Baca, P. Rey, F. Dumeignil, *Green Chem.* **12** (2010) 2079–2098.

[5] C. Garcia-Sancho, J.A. Cecilia, J.M. Merida-Robles, J.S. Gonzalez, R. Moreno-Tost, A. Infantes-Molina, P. Maireles-Torres, *Appl. Catal. B* **221** (2018) 158–168.

[6] Y. Nakagawa, K. Tomishige, *Catal. Sci. Technol.* **1** (2011) 179–190.

[7] D. Sun, Y. Yamada, S. Sato, W. Ueda, *Appl. Catal. B* **193** (2016) 75–92.

[8] Q.H. Sun, S. Wang, H.C. Liu, *ACS Catal.* **7** (2017) 4265–4275.

[9] R. Arundhathi, T. Mizugaki, T. Mitsudome, K. Jitsukawa, K. Kaneda, *ChemSusChem* **6** (2013) 1345–1347.

[33] Y. Nakagawa, X. Ning, Y. Amada, K. Tomishige, *Appl. Catal. A Gen.* **433** (2012) 128–134.

[34] Y. Nakagawa, K. Mori, K. Chen, Y. Amada, M. Tamura, K. Tomishige, *Appl. Catal. A Gen.* **468** (2013) 418–425.

[35] K. Chen, K. Mori, H. Watanabe, Y. Nakagawa, K. Tomishige, *J. Catal.* **294** (2012) 171–183.

[36] Y. Amada, H. Watanabe, M. Tamura, Y. Nakagawa, K. Okumura, K. Tomishige, *J. Phys. Chem. C* **116** (2012) 23503–23514.

[37] Y. Amada, H. Watanabe, Y. Hirai, Y. Kajikawa, Y. Nakagawa, K. Tomishige, *ChemSusChem* **5** (2012) 1991–1999.

[38] S. Liu, M. Tamura, Y. Nakagawa, K. Tomishige, *ACS Sustain. Chem. Engin.* **2** (2014) 1819–1827.

[39] K. Chen, M. Tamura, Z. Yuan, Y. Nakagawa, K. Tomishige, *ChemSusChem* **6** (2013) 613–621.

[40] S. Liu, Y. Okuyama, M. Tamura, Y. Nakagawa, A. Imai, K. Tomishige, *ChemSusChem* **8** (2015) 628–635.

- [41] Y. Nakagawa, M. Tamura, Z. Yuan, K. Tomishige, K. Chen, *ChemSusChem* 6 (2013) 548–548.
- [42] M. Tamura, K. Tokonami, Y. Nakagawa, K. Tomishige, *Chem. Commun. (Camb.)* 49 (2013) 7034–7036.
- [43] M. Tamura, K. Tokonami, Y. Nakagawa, K. Tomishige, *ACS Catal.* 6 (2016) 3600–3609.
- [44] S.B. Liu, S. Dutta, W.Q. Zheng, N.S. Gould, Z.W. Cheng, B.J. Xu, B. Saha, D.G. Vlachos, *ChemSusChem* 10 (2017) 3225–3234.
- [45] S.B. Liu, T. Simonetti, W.Q. Zheng, B. Saha, *ChemSusChem* 11 (2018) 1446–1454.
- [46] M. Mascal, S. Dutta, I. Gandarias, *Angew. Chem. Int. Ed.* 53 (2014) 1854–1857.
- [47] S.B. Liu, T.R. Josephson, A. Athaley, Q.P. Chen, A. Norton, M. Ierapetritou, J.I. Siepmann, B. Saha, D.G. Vlachos, *Sci. Adv.* 5 (2019).
- [48] S. Ito, C. Chibana, K. Nagashima, S. Kameoka, K. Tomishige, K. Kunimori, *Appl. Catal. A Gen.* 236 (2002) 113–120.
- [49] T. Yamagishi, I. Furikado, S. Ito, T. Miyao, S. Naito, K. Tomishige, K. Kunimori, *J. Mol. Catal. A Chem.* 244 (2006) 201–212.
- [50] K. Tomishige, Y. Nakagawa, M. Tamura, *Green Chem.* 19 (2017) 2876–2924.
- [51] Y. Takeda, M. Tamura, Y. Nakagawa, K. Okumura, K. Tomishige, *Catal. Sci. Technol.* 6 (2016) 5668–5683.
- [52] Y. Takeda, M. Tamura, Y. Nakagawa, K. Okumura, K. Tomishige, *ACS Catal.* 5 (2015) 7034–7047.
- [53] S.R. Sashital, J.B. Cohen, R.L. Burwell, J.B. Butt, *J. Catal.* 50 (1977) 479–493.
- [54] Y.G. Chen, K. Tomishige, K. Yokoyama, K. Fujimoto, *J. Catal.* 184 (1999) 479–490.
- [55] J. Okal, *Appl. Catal. A Gen.* 287 (2005) 214–220.
- [56] A.S. Duke, R.P. Galhenage, S.A. Tenney, P. Sutter, D.A. Chen, *J. Phys. Chem. C* 119 (2015) 381–391.
- [57] J.J. Varghese, L. Cao, C. Robertson, Y. Yang, L.F. Gladden, A.A. Lapkin, S.H. Mushrif, *ACS Catal.* 9 (2019) 485–503.
- [58] C.H. Deng, X.Z. Duan, J.H. Zhou, X.G. Zhou, W.K. Yuan, S.L. Scott, *Catal. Sci. Technol.* 5 (2015) 1540–1547.
- [59] L. Zhang, A.M. Karim, M.H. Engelhard, Z.H. Wei, D.L. King, Y. Wang, *J. Catal.* 287 (2012) 37–43.
- [60] R.J. Chimentao, H. Oliva, J. Belmar, K. Morales, P. Maki-Arvela, J. Warna, D.Y. Murzin, J.L.G. Fierro, J. Llorca, D. Ruiz, *Appl. Catal. B* 241 (2019) 270–283.
- [61] F. Sojymosi, T.S. Zakar, *J. Mol. Catal. A Chem.* 235 (2005) 260–266.
- [62] L.E.S. Rygh, I. Gauselmel, O.H. Ellestad, P. Klaeboe, C.J. Nielsen, E. Rytter, *J. Mol. Struct.* 349 (1995) 325–328.
- [63] L.E.S. Rygh, C.J. Nielsen, *J. Catal.* 194 (2000) 401–409.
- [64] W. Daniell, T. Weingand, H. Knozinger, *J. Mol. Catal. A Chem.* 204 (2003) 519–526.
- [65] Y. Ishida, T. Ebashi, S. Ito, T. Kubota, K. Kunimori, K. Tomishige, *Chem. Commun. (Camb.)* (2009) 5308–5310.
- [66] T. Ebashi, Y. Ishida, Y. Nakagawa, S.-i. Ito, T. Kubota, K. Tomishige, *J. Phys. Chem. C* 114 (2010) 6518–6526.
- [67] S. Koso, H. Watanabe, K. Okumura, Y. Nakagawa, K. Tomishige, *Appl. Catal. B* 111 (2012) 27–37.
- [68] O.M. Daniel, A. DeLaRiva, E.L. Kunkes, A.K. Datye, J.A. Dumesic, R.J. Davis, *ChemCatChem* 2 (2010) 1107–1114.
- [69] J. Fusy, M. Alnot, J. Jupille, P. Pareja, J.J. Ehrhardt, *Appl. Surf. Sci.* 17 (1984) 415–428.
- [70] K.G. Azzam, I.V. Babich, K. Seshan, B.L. Mojet, L. Lefferts, *ChemCatChem* 5 (2013) 557–564.
- [71] M. Chia, B.J. O'Neill, R. Alamillo, P.J. Dietrich, F.H. Ribeiro, J.T. Miller, J.A. Dumesic, *J. Catal.* 308 (2013) 226–236.
- [72] K.G. Azzam, I.V. Babich, K. Seshan, L. Lefferts, *J. Catal.* 251 (2007) 163–171.
- [73] Y. Amada, S. Koso, Y. Nakagawa, K. Tomishige, *ChemSusChem* 3 (2010) 728–736.